Contents lists available at ScienceDirect

Petroleum Science

journal homepage: www.keaipublishing.com/en/journals/petroleum-science



Thermal insulation design of subsea vertical X-mas tree

Xin Rong*, Hong-Wu Zhu

College of Mechanical and Transportation Engineering, China University of Petroleum, Beijing, 102249, China



ARTICLE INFO

Article history: Received 31 May 2019 Accepted 24 April 2020 Available online 24 May 2021

Edited by: Xiu-Qiu Peng

Subsea vertical X-mas tree Thermal insulation design Unsteady heat-transfer analysis Computational fluid dynamics

ABSTRACT

Temperature drop is commonly observed in subsea vertical X-mas trees during shutdown. The presence of a huge temperature difference between internal crude oil and external seawater can cause severe equipment degradation of the oil flow channel (e.g., hydrate precipitation), which can block the oil flow channel and interrupt the production process. The most vulnerable parts of a subsea vertical X-mas tree tend to be components with high convective heat transfer rates, such as production modules and short joints. We proposed an innovative approach for the insulation design of underwater equipment under a shutdown condition. First, we obtained a heat transfer analysis of the tree under working conditions through computational fluid dynamics to ascertain the initial temperature condition for an unsteadystate analysis. Second, we investigated the unsteady heat transfer characteristics of the tree with an insulation layer in the shutdown state and derived the relationships between insulation duration and thickness by data analysis. We used data analysis to identify the relationship between insulation duration and thickness. Finally, we derived the empirical formula of insulation thickness for underwater equipment given the effect of environmental factors on the heat preservation effect. We performed the experiment with an oil pipeline, and the results showed that the internal oil of the equipment did not hydrate within 8 h under the shutdown condition with insulation layers.

© 2021 The Authors. Publishing services by Elsevier B.V. on behalf of KeAi Communications Co. Ltd. This is an open access article under the CC BY-NC-ND license (http://creativecommons.org/licenses/by-nc-nd/

4.0/).

1. Introduction

X-mas trees are widely used for offshore oil and gas extraction because of their ability to suspend underground equipment and seal up annular spaces (Minami et al., 1999; Bai, 2019; Davis and Brockhurst, 2015). The structure of the subsea vertical X-mas tree is shown in Fig. 1, and the inner flow channel is presented in Fig. 2. The temperature of internal oil and gas will decrease dramatically during transportation because of the great temperature difference between internal oil and external seawater. For instance, the temperature of 500 m underwater is only 8 °C, whereas the temperature of oil-well outputs can reach up to 120 °C. The presence of temperature drop in oil-well outputs during production may cause flow assurance challenges, such as hydrate formation and wax deposition (Davalath et al., 2002; Gao et al., 2015; Yang et al., 2015). In other words, insulation measures must be taken for efficient production.

Analysis of heat transfer performance to the tree acts as the first step in heat preservation design. Zabaras and Zhang (1997)

* Corresponding author.

E-mail address: 2018314008@student.cup.edu.cn (X. Rong).

analyzed the thermal performance of subsea trees under steady and unsteady states and proved the necessity for insulation design. Dwight et al. (2004) investigated the effect of boundary conditions on computational accuracy. Their results indicated that the convective heat transfer of the internal oil can be overlooked in thermal analysis of the underwater tree. This finding can be explained by the fact that under stable conditions, the temperature of the inner wall of the flow channel remains consistent with that of crude oil, which can be treated as a constant temperature boundary. Under unsteady conditions, the limited heat existing in internal crude oil can slightly affect the heat transfer of the overall system.

As for research methods, Sorbye and Moe (2006) reported that the heat transfer analysis conducted by computational fluid dynamics (CFD) was more accurate than that by finite element analysis (FEA), and the same conclusion was also drawn by Lu et al. (2.011).

Some scholars have studied the duration of the insulation layer. Rivas-Cardona et al. (2013) analyzed the insulation performance of the pipeline under a shutdown state. They found that the CFD method could effectively predict the length of time required for crude oil inside the equipment to cool to the critical temperature (the temperature at which hydrates are appears). In addition, CFD

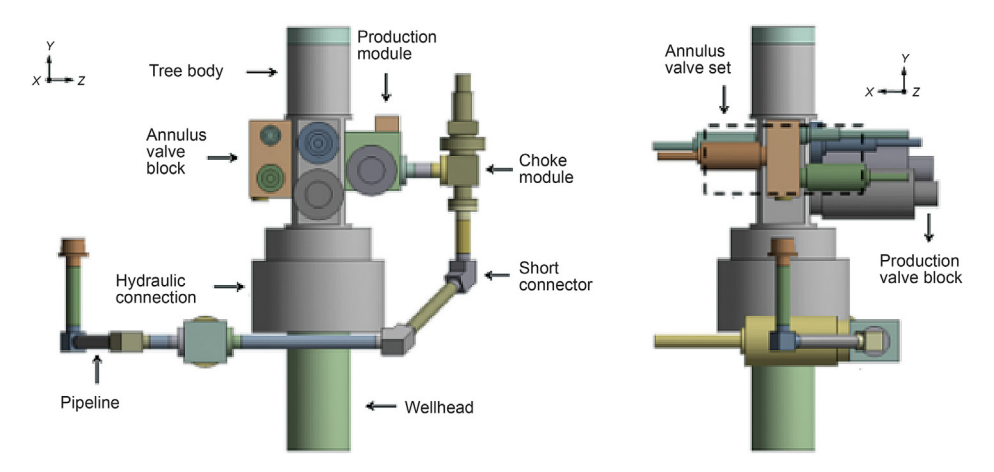


Fig. 1. Structure and components of subsea vertical X-mas tree assembly.

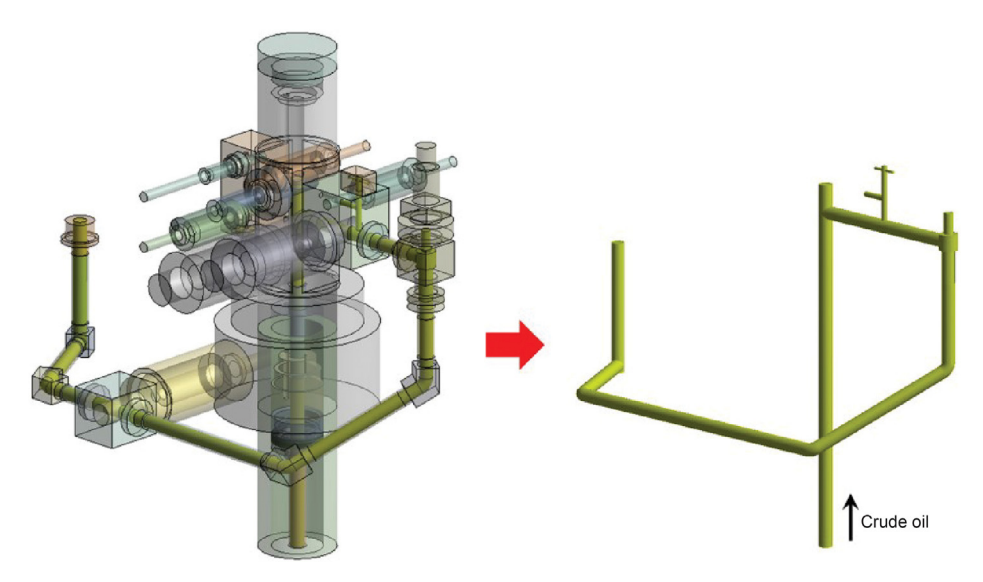


Fig. 2. Inner flow channel of subsea vertical X-mas tree.

can identify the weak position of insulation and provide a reference for thermal insulation design.

We proposed a method for the thermal insulation design of subsea X-mas trees; the flow chart of our research method is shown in Fig. 3. The purpose was to ensure that the internal oil of the equipment would not freeze within 8 h after shutdown. The critical temperature was 23 °C (the freezing point of Shengli crude oil). Using the CFD method, we studied the steady and unsteady heat transfer characteristics of subsea vertical trees at 500 m underwater and derived a formula for the thickness of the insulation layer by data analysis. The cool-down process of internal crude oil in subsea vertical trees is a complex phenomenon affected by different factors, including seawater temperature, fluid velocities, seawater flow direction, and oil temperature. In abyssal environments, water temperature is relatively stable and can act as a constant. For instance, the sea temperature is nearly 8 °C at 500 m underwater, and the water flow rate can range from 0.2 m/s to 0.8 m/s. As for seawater flow direction, different orientations refer to different heat transfer characteristics. It also has been proven that the oil temperature drop rate is the fastest under installation orientation 1, as shown in Fig. 4 (Frank et al., 2008; Singh et al., 2014; Hu et al., 2015), and in call cases, the temperature of seawater was 8 °C. The following sections discuss the influence of oil temperature and seawater flow rate.

2. Insulation form and material selection

A multilayer structure is applied primarily in equipment with a simple structure, such as submarine pipeline. For complicated components of a subsea tree, we adopted a single-layer insulation.

The common material exhibiting a thermal conductivity of less than 0.2 W/m·°C generally refers to the insulating material. In a deep-water environment, however, for external environments with low temperature and high pressure, and considering the inevitable collision and impact that occurs during installation and maintenance, the insulation material should exhibit good insulation properties, low water absorption, and high mechanical properties (Chen et al., 2012; Susan et al., 2013; Shubham et al., 2019; Xu et al., 2019). The common insulation materials and their properties are listed in Table 1 (Caputo et al., 2015; Koosha and Newsha, 2020; Modeste et al., 2015). Given the cost and manufacturing difficulty, we used integral polyurethane as the insulation material.

3. Methodology

3.1. Geometric model

3.1.1. Model for steady heat transfer analysis

Fig. 5 illustrates the computational model for steady-state

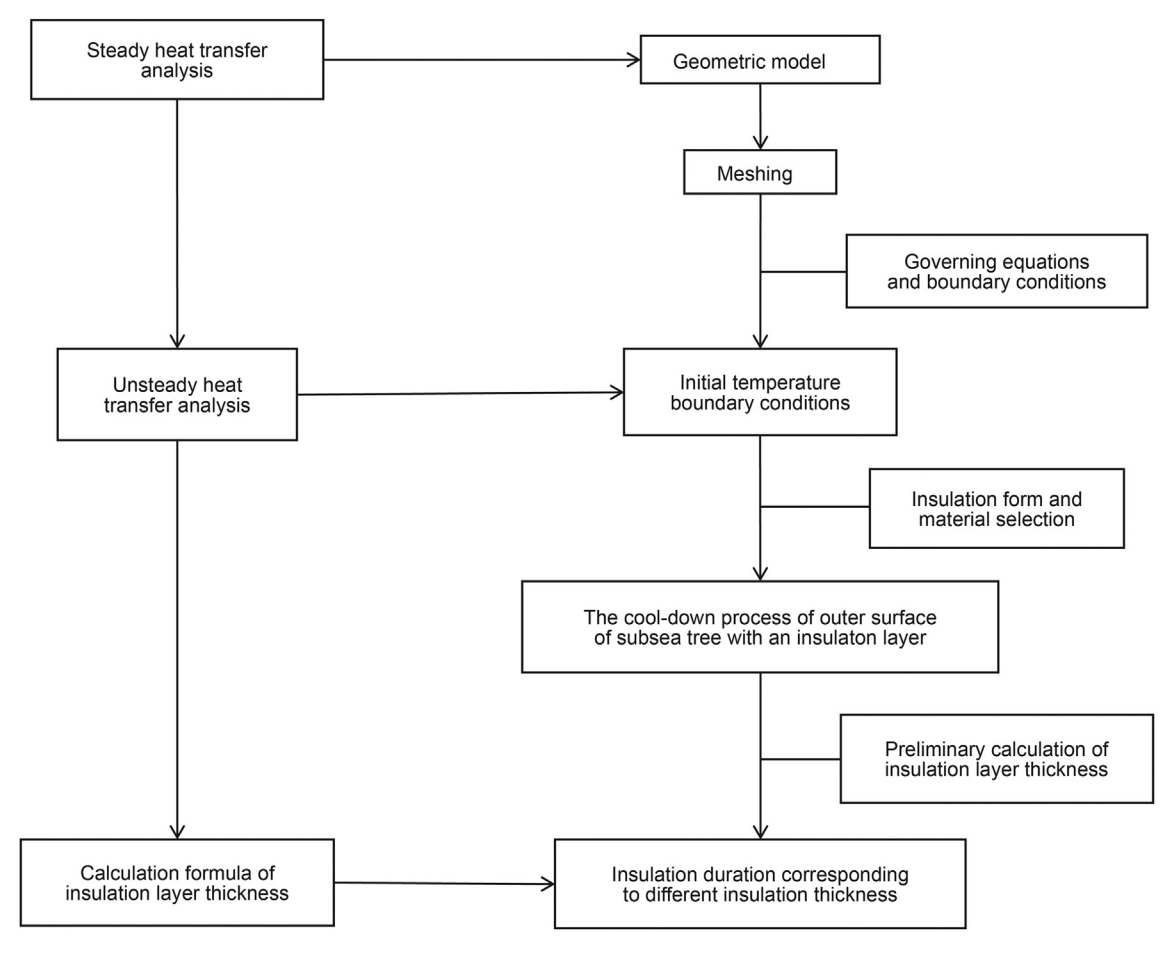


Fig. 3. Flow chart of insulation design.

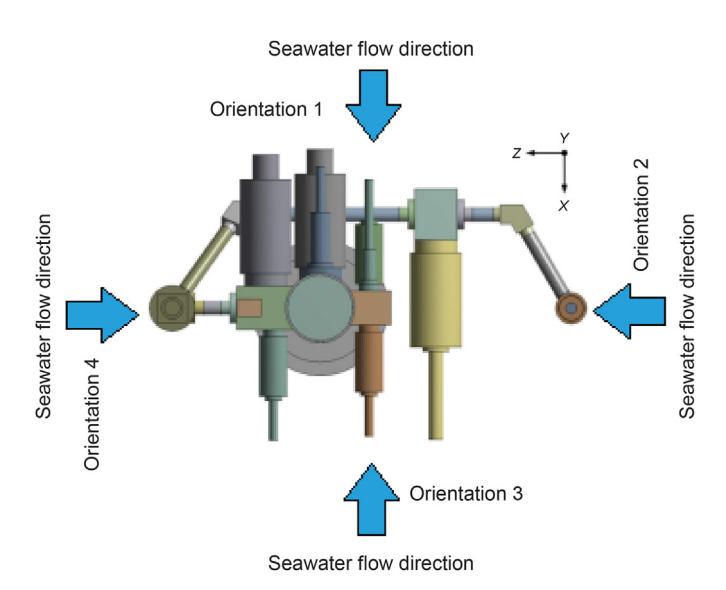


Fig. 4. Four orientations for vertical subsea vertical X-mas tree assembly.

transfer of the subsea vertical X-mas tree. The entire model consists of fluid domains of internal crude oil and external seawater and a solid domain of the tree. The size of the tree is $l \times w \times h = 5 \times 3 \times 5$ m, and the entire calculation domain is $L \times W \times H = 25l \times 7w \times 4h$ (Chen et al., 2004; Ratnam and

Vengadesan, 2008). To eliminate the effect of exit boundary on sea flow field, we set the distance from the tree to the inlet to 10 times l and 25 times l to outlet.

3.1.2. Model for unsteady heat transfer analysis

The geometry of the subsea vertical X-mas tree with an insulation layer is shown in Fig. 6. Due to complex geometry, the generation of 3D unstructured mesh of tetrahedrons was easier compared to structured mesh comprising of hexahedrons. The computational domain was divided with a block-structured grid of 4,260,000 tetrahedral cells. The grid resolution was finer in critical regions (e.g., production modules, tree body, choke modules, oil pipeline, and short joint).

3.2. Governing equations

3.2.1. Equations for steady heat transfer analysis

We considered the internal oil and external cold water to be three-dimensional, in-compressible stable fluid. For the internal confined space of the tree, we introduced the Boussinesq hypothesis to process the natural convection attributed to the lift force (Lei et al., 2008). We considered density to be a variable regardless of the viscous dissipation of the fluid. We added volume-related content to the momentum equation, but we treated the density of other regions as a constant.

The corresponding governing equations are described as follows:

Table 1Common external insulation materials.

Name	Maximum temperature, °C	Water absorption	Density, kg/m ³	Maximum water depth, m	Thermal conductivity, W/ m.°C	Advantage	Disadvantage
Composite polypropylene	115	< 1%	650-750	1500	0.15-0.18	Good toughness, no water depth limit	115 °C or higher cannot be used, high cost
Integral polyurethane	115	< 1%	780-850	Unlimited	0.18-0.22	Good thermal insulation and toughness	115 °C or higher cannot be used
Silicone Rubber	350	< 10%	1080	Unlimited	0.19-0.20	Good toughness, high temperature resistance	High density, high price
Composite silicone resin	150	< 10%	750-850	3000	0.15-0.18	Good toughness, high temperature resistance	High price
Composite epoxy resin	120	< 0.5%	700850	3000	0.100.135	Good thermal insulation	Poor toughness, high construction difficulty
Complex phenolic	200	< 5%	750-850	3000	0.018 - 0.21	High temperature resistance	High cost, high pollution
Vacuum Insulation Pane	70	< 0.5%	240-314	_	0.004	Good insulation	High cost, low toughness
Aerogel	1200	< 0.5%	3-600	1500	0.011-0.015	High temperature resistance	High cost
Extruded Polystyrene Board	70	< 1%	25–32	-	0.028-0.03	Good thermal insulation, low density	High cost

Note: The mentioned values were measured at an average production temperature of 50 $^{\circ}$ C.

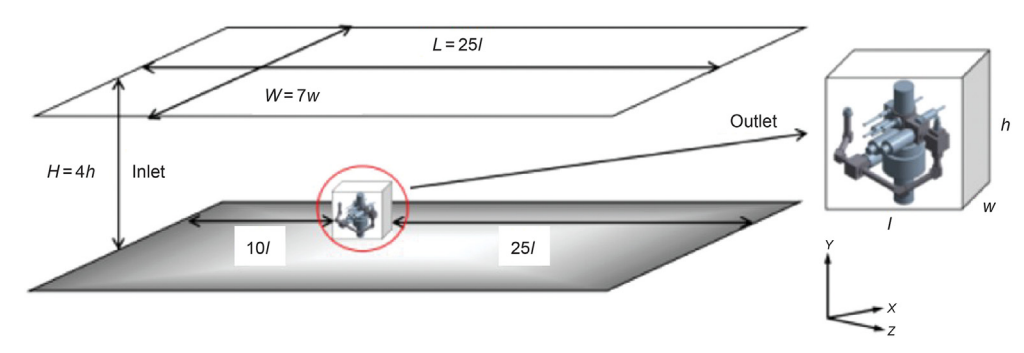


Fig. 5. Computational model of the subsea vertical X-mas tree.

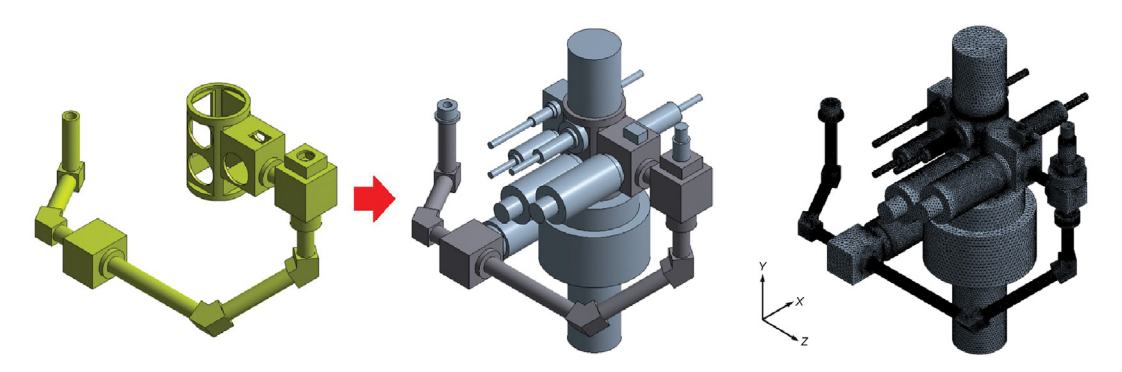


Fig. 6. Structure of insulation layer of subsea vertical X-mas tree and meshing result.

Continuity equation:

$$\nabla \cdot (\rho u V) = -\frac{\partial p}{\partial y} + \frac{\partial}{\partial y} \left(\mu \frac{\partial v}{\partial y} \right)$$

$$\text{Z-momentum equation:}$$
(3)

X-momentum equation:

$$\nabla \cdot (\rho u V) = -\frac{\partial p}{\partial x} + \frac{\partial}{\partial x} \left(\mu \frac{\partial u}{\partial x} \right) \tag{4}$$

Y- momentum equation: Momentum equation complying with the Boussinesq hypothesis (for internal confined spaces):

$$\nabla \cdot (\rho uV) = -\frac{\partial p}{\partial x} + \frac{\partial}{\partial x} \left(\mu \frac{\partial u}{\partial x} \right) + \rho g \beta (T - T_0)$$
(5)

Energy equations (covering solid and fluid domains):

$$\nabla \cdot (C_{P}\rho TV) = \nabla \cdot (\lambda \nabla T) \tag{6}$$

where ρ denotes density, kg/m³; V is velocity vector; p is pressure, Pa; μ is dynamic viscosity, Pa·s; β is thermal expansion coefficient, 1/°C; g is gravitational acceleration, m/s²; T is temperature, °C; T0 indicates ambient temperature, °C; λ is thermal conductivity, W/m·°C; and C0 is specific heat capacity, J/Kg·°C.

3.2.2. Equations for unsteady heat transfer analysis

To analyze the unsteady heat transfer of three-dimensional incompressible fluid, the governing equations are shown in Eqs. (7)–(9).

Continuity equation:

$$\frac{\partial \rho}{\partial t} + \nabla \cdot (\rho V) = 0 \tag{7}$$

The momentum equation complying with the Boussinesq hypothesis in the direction of gravity:

$$\frac{\partial(\rho\nu)}{\partial t} + \nabla \cdot (\rho u V) = -\frac{\partial p}{\partial y} + \frac{\partial}{\partial y} \left(\nu \frac{\partial u}{\partial y} \right) + \rho g \beta (T - T_0)$$
(8)

Energy equations (including solid and fluid domains):

$$\frac{\partial(\rho T)}{\partial t} + \nabla \cdot (C_{P}\rho TV) = \nabla \cdot (\lambda \nabla T) \tag{9}$$

3.3. Boundary conditions

3.3.1. Conditions for steady heat transfer analysis

For external cold water, we took the velocity inlet $(u=u_{\rm in}, v=0, w=0, T_0=8$ °C) and the free flow outlet $(\partial u/\partial x=\partial v/\partial y=\partial w/\partial z=\partial T/\partial x=0)$ as boundary conditions and set all walls to be nonslip and adiabatic. For internal crude oil, we adopted the velocity inlet boundary $(v=0.2 \text{ m/s}, T=T_{\rm in})$ and the free outflow exit boundary as well. We coupled the inner and outer walls of the tree with the inner and outer fluid, respectively, and all were set to no slip wall, regardless of the effect of surface roughness.

3.3.2. Conditions for unsteady heat transfer analysis

The temperature result of steady state of the tree acted as the initial condition for the calculation of the unsteady-state analysis:

$$T = f(x, y, z) \tag{10}$$

We set the inlet and outlet of the internal crude oil to the adiabatic boundary ($q_W = 0$) and altered the physical properties of the crude oil (taken from Daqing oilfield) by user-defined function (UDF) programming as the temperature decreased. Physical properties of crude oil were shown in Table 2.

For the high thermal resistance of the insulation layer, the temperature of the external surface of the insulation layer was low, so the heat loss resulting from the convection heat transfer of the external seawater was extremely small. Thus, overlooking the heat loss in this part, we considered the outside temperature of the insulation layer to be constant ($T_{\rm surf} = T_{\rm sea}$). For noninsulated parts, we applied a third type of thermal boundary onto their outer surfaces:

$$-\lambda_{s} \frac{\partial T}{\partial n} = h_{\text{CHTC}} \left(T_{\text{surf}} - T_{\text{sea}} \right) \tag{11}$$

where

$$h_{\text{CHTC}} = \frac{\Phi}{A \left(T_{\text{surf}} - T_{\text{sea}} \right)} \tag{12}$$

where λ_s denotes the thermal conductivity of material AISI 8630 (the common material for the subsea vertical X-mas tree), W/m·°C; h_{CHTC} is the average convective heat transfer coefficient of external surface of respective component (Hu et al., 2016), W/m²·°C; Φ is the amount of heat loss, W; A represents the surface area of various components, m²; T_{surf} is the surface temperature, °C; and T_{sea} is the external seawater temperature, °C.

During unsteady analysis, we adopted the SIMPLE algorithm to solve the coupling problem of pressure and velocity and took the second-order upwind style to separate the momentum equation, energy equation, and turbulent kinetic energy equation. For the temperature drop calculation, the time step was 0.1 s for 0-60 s, 0.5 s for 0-60 s to 0.5 s for 0.5 s fo

3.4. Numerical methods

We employed the realizable k- ϵ turbulence model and the low Reynolds number model to solve the heat transfer problem of the subsea vertical X-mas tree (Hu et al., 2016). The turbulent kinetic energy and dissipation rate transport equations can be expressed as follows:

$$\frac{\partial(\rho k)}{\partial t} + \frac{\partial(\rho k u_i)}{\partial x_i} = \frac{\partial}{\partial x_j} \left[\left(\mu + \frac{\mu_t}{\sigma_k} \right) \frac{\partial k}{\partial x_j} \right] + G_k + G_b - \rho \varepsilon - Y_M \tag{13}$$

Table 2 Physical properties of crude oil used in UDF.

Property	Expression	Temperature range
Density, kg/m ³	$\rho = 840$	30 °C ≤ T ≤ 110 °C
Heat capacity, J/kg.°C	$C_{\rm p} = 3647.811 + 16.987T - 1.01T^2$	30 °C ≤ T < 52 °C
	$C_{\rm p} = 1794.969 + 3.607T$	$52~^{\circ}\text{C} \leq T \leq 110~^{\circ}\text{C}$
Heat conductivity, W/m·°C	$\lambda = 0.60576 - 0.01186T$	$30~^{\circ}\text{C} \leq \text{T} < 48~^{\circ}\text{C}$
	$\lambda = 0.152 \exp(-9.18 \times 10 - 4T)$	48 °C \leq T \leq 110 °C
Dynamic viscosity, Pa·s	$\mu = 10^{3.887948 - 0.12235T}$	30 °C ≤ T < 48 °C
	$\mu = 10^{-(0.26877 + 0.01951T)}$	48 °C ≤ T ≤ 110 °C

$$\begin{split} &\frac{\partial(\rho k)}{\partial t} + \frac{\partial(\rho k u_i)}{\partial x_i} = \\ &\frac{\partial}{\partial x_j} \left[\left(\mu + \frac{\mu_t}{\sigma_{\varepsilon}} \right) \frac{\partial \varepsilon}{\partial x_j} \right] + \rho C_1 E \varepsilon - \rho C_2 \frac{\varepsilon^2}{k + \sqrt{\nu \varepsilon}} + C_{1\varepsilon} \frac{\varepsilon}{k} C_{3\varepsilon} G_b \end{split} \tag{14}$$

where

$$\begin{split} C_1 &= \text{max}\Big(0.43, \frac{\eta}{\eta+3}\Big), \eta = \big(2E_{ij} \cdot E_{ij}\big)^{\frac{1}{2}} \frac{k}{\varepsilon} \\ E_{ij} &= \frac{1}{2} \left(\frac{\partial u_i}{\partial x_j} + \frac{\partial u_j}{\partial x_i}\right), \mu_t = \rho C_\mu \frac{k^2}{\varepsilon} \\ C_\mu &= \frac{1}{A_0 + A_S U^* k/_S}, A_S = \sqrt{6} \text{cos } \varphi \\ &\qquad \qquad - \varepsilon_{ijk} \varpi_k \\ \varphi &= \frac{1}{3} \text{cos}^{-1} \Big(\sqrt{6} \, W\Big), W = \frac{E_{ij} E_{jk} E_{kj}}{\big(E_{ij} E_{ij}\big)^{\frac{1}{2}}} \\ U^* &= \sqrt{E_{ij} E_{ij} + \tilde{\Omega}_{ij} \tilde{\Omega}_{ij}} \\ \tilde{\Omega}_{ij} &= \Omega_{ij} - 2\varepsilon_{ijk} \varpi_k, \overline{\Omega_{ij}} \end{split}$$

where G_k denotes the generation of turbulent kinetic energy attributed to the average velocity gradient; G_b is the turbulent energy generated by the buoyancy effect; Y_M is the effect of the compressible turbulent pulsation expansion on the total dissipation rate; $C_{1\epsilon}$, $C_{2\epsilon}$, $C_{3\epsilon}$, C_2 , and A_0 are the empirical constant, and their default values in FLUENT are $C_{1\epsilon}=1.44$, $C_{2\epsilon}=1.9$, $C_{3\epsilon}=0.09$, $C_2=1.9$, and $A_0=4.0$, respectively; and σ_k and σ_ϵ are the Prandtl numbers corresponding to the turbulent kinetic energy and the turbulent dissipation rate, respectively, with the default values of $\sigma_k=1.0$, $\sigma_\epsilon=1.2$.

4. Numerical simulation results and analysis

4.1. Temperature drop of subsea tree without insulation

We studied the temperature of a subsea vertical X-mas tree under the shutdown condition by numerical simulation. Fig. 7 shows the temperature distribution for the tree without insulation. We obtained data while the initial temperatures of the crude oil and seawater were 120 $^{\circ}$ C and 8 $^{\circ}$ C, respectively.

We observed that the temperature was significantly higher for the oil pipeline than for other components at the beginning. After 30 min of shutdown, however, the surface temperature of the oil pipeline was significantly lower than other components, such as production modules and pipeline gate valves. We attributed this lower temperature to different convection heat transfer coefficients on the outer surface of different parts. For the oil pipeline, the temperature drop rate was faster than other areas because of the higher convection heat transfer coefficient (Hu et al., 2015).

In Fig. 8, the average temperatures for oil pipeline are plotted against length of downtime ranging from 0 to 80 min. The considerable decrease in temperature at the beginning is evident. The temperature dropped sharply from $14.6~^{\circ}\text{C}$ to $10.4~^{\circ}\text{C}$ in the first 3 min and then decreased slowly for the next 30 min. Eventually, the temperature of the outer wall was close to that of the seawater.

In all cases, the critical temperature was 23 °C (the freezing point of Shengli crude oil). In other words, if the crude oil temperature was lower than 23 °C, problems such as wax precipitation and hydrate formation could damage the equipment and interrupt the process of oil extraction.

We applied the volume-averaged temperature of crude oil for this research to avoid the influence caused by the uneven temperature distribution of crude oil in axial and radial directions. Fig. 9 shows the cool-down process of crude oil in a subsea X-mas tree. We observed that the temperature of crude oil dropped from 120 °C to 50 °C in the first 25 min, whereas the temperature

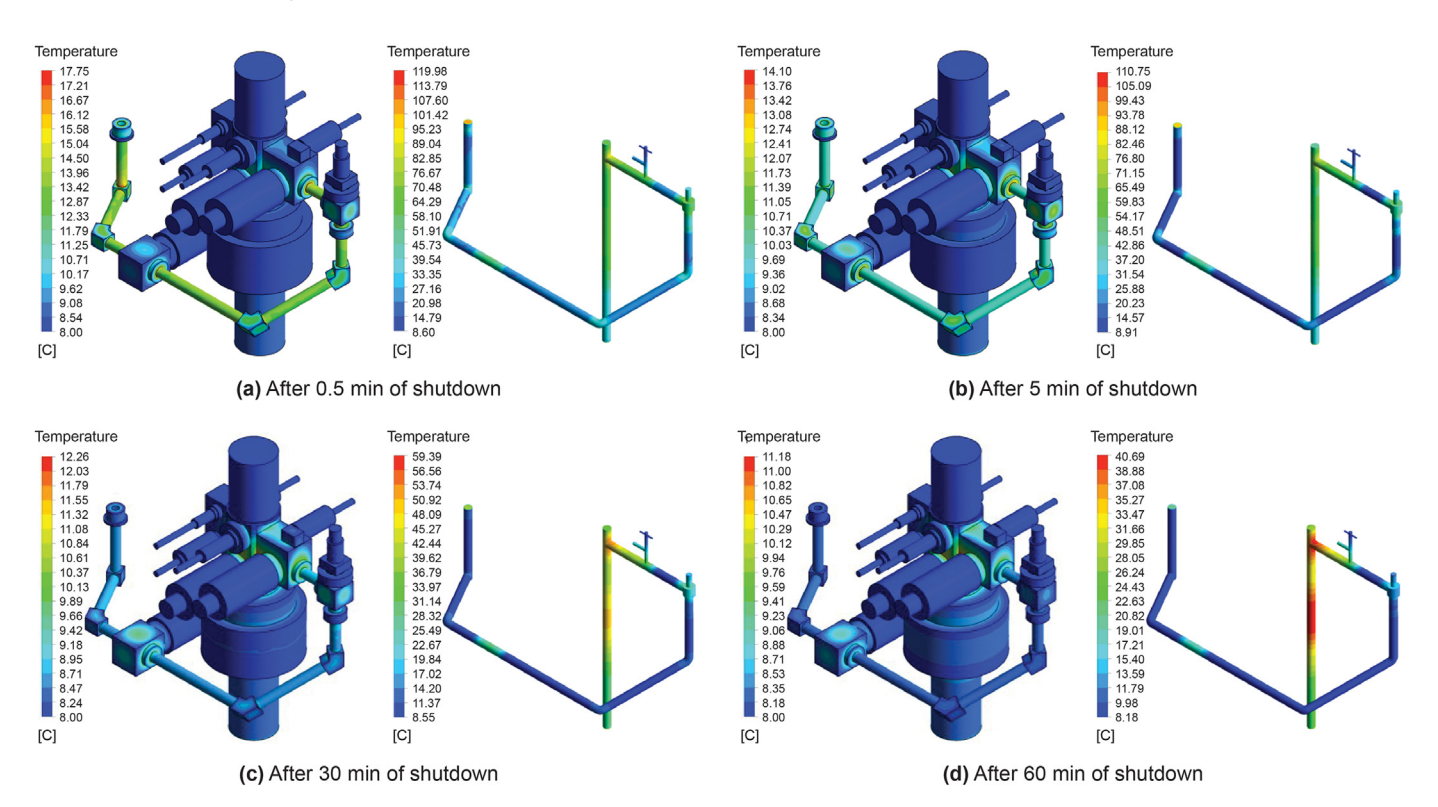


Fig. 7. Cool-down process of subsea vertical X-mas tree.

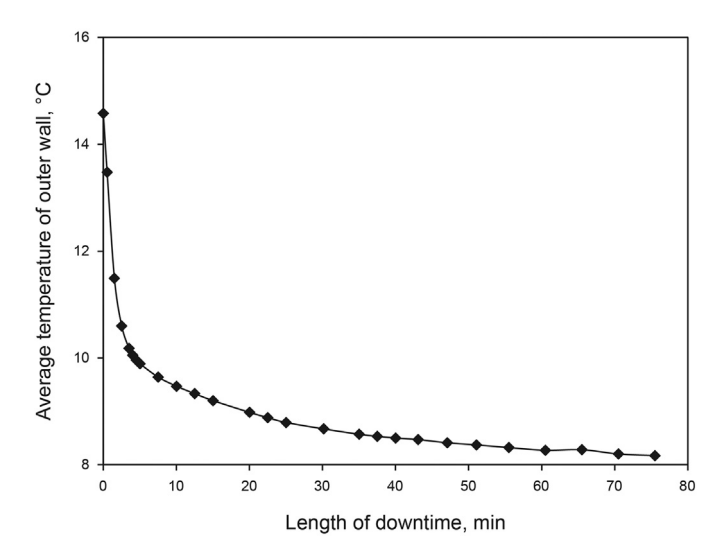


Fig. 8. Cool-down process of surface of pipeline.

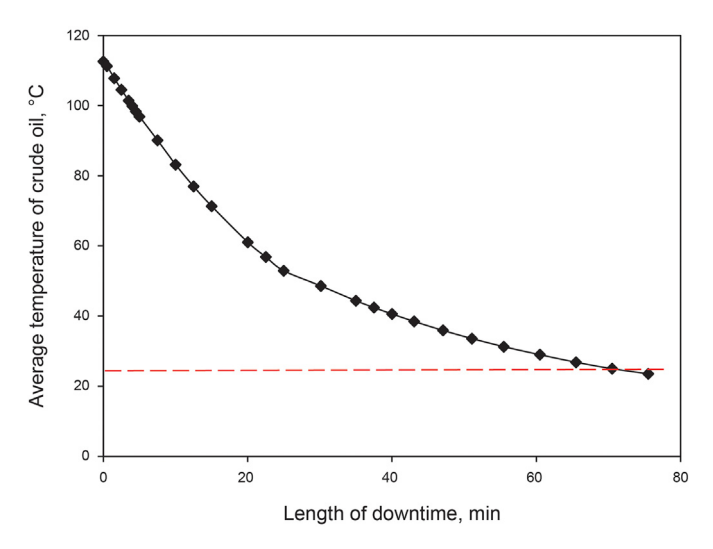


Fig. 9. Cool-down process of crude oil in subsea X-mas tree.

dropped only by 30 °C in the next 50 min. About 75 min after shutdown, the average temperature of the crude oil dropped to 23 °C, reaching the critical value. This was far from meeting the engineering requirement of no hydrate formation within 8 h after shutdown. Therefore, it would be necessary to add an insulation layer to the subsea vertical X-mas tree.

4.2. Temperature drop of subsea tree with insulation

4.2.1. Preliminary calculations and simulation results

To account for environmental differences between land and sea, the conventional insulation thickness calculation formula should be adopted only for the preliminary calculation of the subsea tree insulation design. Accordingly, we exploited the trial-and-error method (Montazeriab and Blockena, 2018) to ascertain the thickness of the insulation layer. First, based on the preliminary calculation results, we built a three-dimensional calculation model with an insulation layer. Subsequently, we obtained the maximum insulation duration corresponding to different thicknesses by numerical simulation. Next, we determined the relationships between insulation duration and insulation thickness by data analysis.

Finally, we derived the thickness of the insulation layer satisfying the requirement of 8 h insulation.

We adopted the thermal equilibrium method for preliminary calculation (Wu, 1986). Referencing the Thermal Engineering Design Manual (Wu, 1986), the formula can be expressed as follows:

$$\begin{cases}
\ln \frac{D_{1}}{D_{0}} = \frac{7200\pi\lambda_{i} \left(\frac{T_{0} + T_{fr}}{2} + T_{sea}\right) \cdot t_{fr}}{\left(T_{0} - T_{fr}\right) \left(V\rho C + V_{p}\rho_{p}C_{p}\right)} - \frac{2\lambda_{i}}{D_{1}h_{CHTC}} \\
\delta = \frac{1}{2}(D_{1} - D_{0})
\end{cases} (15)$$

where D_0 denotes the outer diameter of the pipeline, m; D_1 is the outer diameter of the insulation layer, m; λ_i is the thermal conductivity of the insulation material, $W/(m\cdot^{\circ}C)$; T_0 is the oil start temperature, ${}^{\circ}C$; T_{fr} is the oil critical temperature, ${}^{\circ}C$; T_{sea} is the seawater ambient temperature, ${}^{\circ}C$; t_{fr} refers to the residence time of crude oil in the pipeline without freezing, h; t_{CHTC} represents the heat transfer coefficient of external seawater, t_{CHTC} represents the heat volume of crude oil and wall, respectively, t_{CHTC} and t_{CHTC} represents the density of crude oil and wall, respectively, t_{CHTC} and t_{CHTC} indicate the heat capacity of crude oil and wall material, respectively, t_{CHTC} is and t_{CHTC} is the thickness of insulation layer, m.

The thickness δ of the insulation layer should be set before calculating the value of D_1 in Eq. (15), and the calculation is conducted according to Eq. (16).

The initial temperature of internal crude oil was 40 °C with a flow rate of 0.2 m/s, and the external seawater temperature was 8 °C with a flow rate of 0.8 m/s. With integral polyurethane (thermal conductivity: 0.2 W/($m \cdot ^{\circ}C$)) as the heat insulating material, we entered the relevant parameters into Eq. (16), and the thickness of the insulating layer was obtained as 0.0405 m. We built a three-dimensional insulation layer model with a tree body, production, throttling oil pipeline, and short joint, as follows:

$$\begin{cases}
\ln \frac{D_{1}}{D_{0}} = \frac{7200\pi\lambda_{i} \left(\frac{T_{0} + T_{fr}}{2} + T_{sea}\right) \cdot t_{fr}}{\left(T_{0} - T_{fr}\right) \left(V\rho C + V_{p}\rho_{p}C_{p}\right)} - 2\pi\lambda_{i}R_{0} \\
\delta = \frac{1}{2}(D_{1} - D_{0})
\end{cases} (16)$$

The steady calculation results are presented in Fig. 10. The figure shows that the temperature of the outer surface of the entire tree was low, which was similar to the temperature of the sea. The only parts that were not insulated (e.g., production valve group) had a temperature that was slightly higher than the seawater temperature, which was significantly different from the case without the insulation layer (Hu et al., 2015). This result indicated that the application of external insulation effectively prevented the heat loss inside the tree.

On the basis of the stable heat transfer analysis, we conducted a nonsteady heat transfer analysis to verify whether the external insulation layer could effectively ensure that the internal crude oil temperature was higher than the critical value in 8 h under the shutdown scenario. Fig. 10 shows the temperature distribution of the subsea vertical X-mas tree with insulation under a working condition. The cool-down process of the average body temperature of the crude oil inside the tree is presented in Fig. 11.

It was evident that when the initial oil temperature was $40\,^{\circ}$ C and the seawater flow rate was $0.8\,$ m/s, the $40.5\,$ mm thick insulation layer could keep the temperature of the internal oil above the critical value of $23\,^{\circ}$ C for only $2.13\,$ h after shutdown, which was far

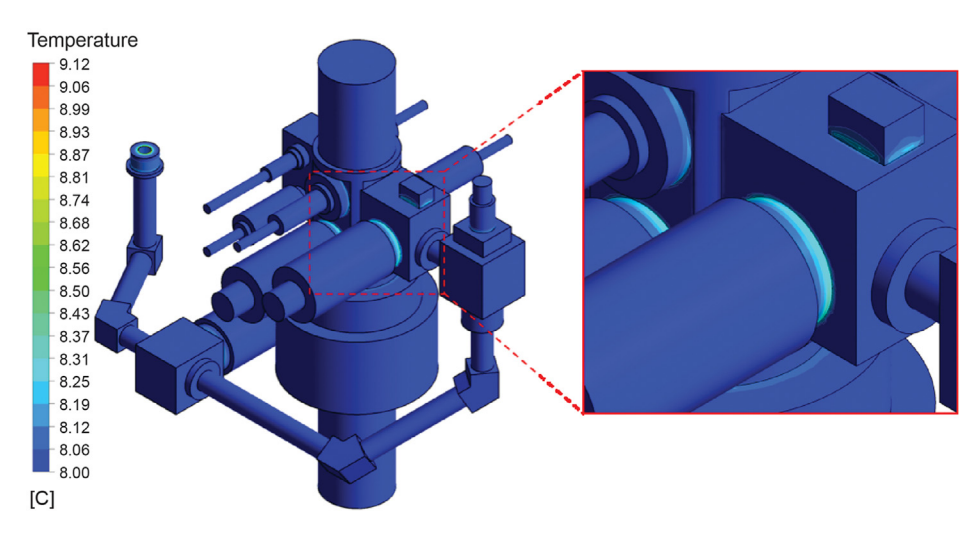


Fig. 10. Temperature distribution of subsea vertical X-mas tree with insulation in the working condition.

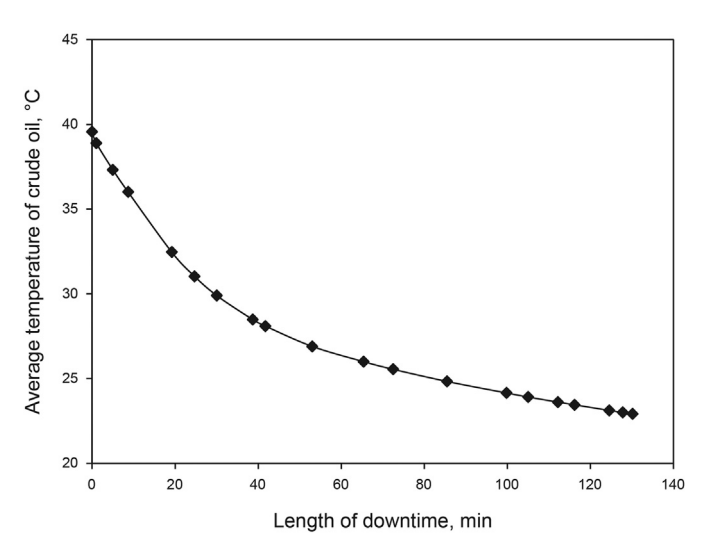


Fig. 11. Cool-down process of crude oil in subsea vertical X-mas tree with insulation in the shutdown condition.

from the 8 h requirement. Thus, the thickness of insulation layer should be enhanced.

The insulation duration for insulation thickness of 70.5 mm, 110.5 mm, and 150.5 mm were 3.45 h, 5.15 h, and 6.89 h, respectively. Fig. 12 gives the maximum heat preservation time of the insulation layers with different thicknesses. The relationships between the two can be expressed as follows:

$$t = 0.0432\delta + 0.3879 \tag{17}$$

where t denotes the maximum holding time, h; and δ is the thickness of the insulating layer, mm.

The correlation coefficient R^2 of Eq. (17) was 99.8%, and uncertainty $u(y_0)$ was 2.53 mm, according to Eq. (18).

$$R^{2} = \frac{\sum_{i=1}^{n} x_{i} \cdot y_{i} - nxy}{\sqrt{\left[\sum_{i=1}^{n} x_{i}^{2} - n\overline{x}\right] \cdot \left[\sum_{i=1}^{n} y_{i}^{2} - n\overline{y}^{2}\right]}}$$
(18)

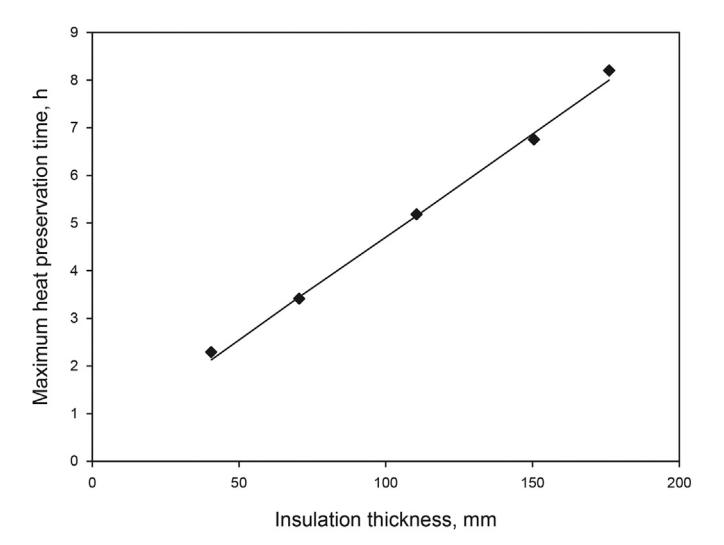


Fig. 12. Maximum heat preservation time of insulation layers with different thicknesses.

$$s_{R} = \sqrt{\frac{\sum_{i=1}^{n} (y_{i} - (bc_{i} + a))^{2}}{n-2}}$$

$$u(y_0) = s(y_0) = s_R \sqrt{\frac{1}{p} + \frac{1}{n} + \frac{(\overline{x_0} - \overline{x})^2}{\sum_{i=1}^{n} (x_i - \overline{x})^2}}$$

We compared the simulation data with the calculated results obtained by Eq. (17). As shown in Table 3, the maximum error of Eq. (17) was only -0.48%. Consequently, we assumed that this formula accurately predicted the heat preservation time. According to Eq. (17), the thickness of the polyurethane insulation layer should be at least 176.17 mm to ensure that the internal oil temperature will not drop to 23 $^{\circ}\text{C}$ in 8 h after shutdown.

4.2.2. Formula for calculating the thickness of insulation layer

Actually, a small variation in external seawater flow rate and initial temperature of crude oil can result in a meaningful change

Table 3Maximum heat preservation time obtained by simulation and Eq. (17).

Insulation thickness	Maximum heat preservation time	Relative error	
δ, mm	Simulation results t_s , h	Formula results $t_{\rm f}$, h	η, %
40.5	2.13	2.14	0.35
70.5 110.5	3.45	3.43	-0.48
110.5	5.15	5.16	0.22
150.5	6.89	6.89	-0.01

on the heat performance of the tree (Hu et al., 2015). Consequently, we investigated the effect of these two factors on insulation performance.

(1) Influence of seawater velocity

Table 4 presents the maximum heat preservation time of insulation under different layers. We observed a considerable increase in the convective heat transfer coefficient of the external surface for various components when the seawater velocity increased (Hu et al., 2015).

The influence of seawater velocity, however, was small. In other words, when seawater velocity increased from the 0.2~m/s to 0.8~m/s, the maximum holding time decreased by 1.87% and 1.97% for the insulation layer thicknesses of 40.5~mm and 150.5~mm, respectively. We attributed this to the fact that in the case of heat preservation, the surface temperature of the tree was not significantly different from the seawater, even if the heat transfer coefficient of the outer surface of the tree increased with the increase in seawater flow velocity. The ratio of heat loss resulting from the external convection heat transfer to the total heat loss remained small, revealing that the effect of the seawater flow rate on insulation performance could be overlooked in research.

(2) Effect of initial temperature of crude oil

When the seawater flow rate was 0.8 m/s and the initial oil temperature was 40 °C, 60 °C, 80 °C, 100 °C, and 120 °C, the thickness of the insulation layer required for the subsea vertical X-mas tree should reach 176.17 mm, 68.31 mm, 32.73 mm, 23.42 mm, and 20.27 mm, respectively. Fig. 13 shows the relationship between insulation layer thickness and initial temperature of crude oil. The relationship between them is described as follows:

$$\delta = 9 \times 10^{-6} {T_0}^4 - 0.0036 {T_0}^3 + 0.5449 {T_0}^2 - 37.29 {T_0} + 1002.3 \tag{19} \label{eq:delta_fit}$$

The correlation coefficient R^2 of Eq. (19) was 93.8%, and uncertainty $u(y_0)$ was 4.84 mm, according to Eq. (18).

Table 5 presents the insulation thicknesses calculated by simulation and formula. The maximum error of Eq. (19) was only -4.78%, which indicated that the formula accurately predicted the thickness of the insulation layer. In brief, because the current seawater velocity slightly affected insulation duration, the initial

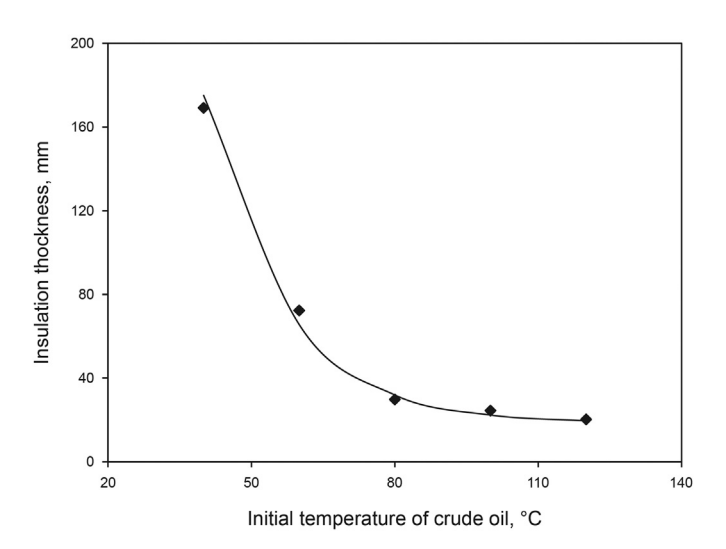


Fig. 13. Adequate thicknesses of the insulation layer corresponding to different initial temperatures of crude oil.

crude oil temperature acted as the only factor affecting the holding time of the insulation layer. Accordingly, we adopted Eq. (19) as an empirical formula for the thickness of the insulation layer for subsea X-mas trees.

5. Validation study

5.1. Experimental setup

To verify the feasibility of insulation empirical formula, we performed an oil pipeline test. As the fastest heat-dissipating component in the tree, the validation test using the oil pipeline was the most convincing (Aarnes et al., 2005; Qin et al., 2011). Fig. 14 illustrates the insulation experimental system. The test bench consisted of a water tank, a hot oil circulation system, a section of oil pipeline with an insulation layer, and a data acquisition system. The hot oil circulation system included the pipeline, constant temperature oil bath (0 °C–200 °C, accuracy±0.1 °C, capacity 30 L, oil pump maximum flow rate 30 L/min), turbine flow meter (DN 32), and two ball valves. To reduce the loss of heat during circulation, we introduced an insulation layer to the piping of the system.

Table 4Maximum heat preservation time of insulation layers in the case of two current velocities.

Insulation layer thickness	Maximum holding time t , min		Difference, %
δ, mm	Seawater flow rate of 0.2 m/s	Seawater flow rate of 0.8 m/s	
40.5	130.16	127.77	1.87
70.5	211.51	207.05	2.15
110.5	314.47	309.26	1.68
150.5	421.52	413.39	1.97

Table 5
Insulation thickness calculated by simulation and formula

Initial oil temperature	Insulation thickness		Relative error
T_0 , °C	Simulation results $\delta_{ m s}$, mm	Formula results $\delta_{ m f}$, mm	η, %
40	176.17	175.18	-0.56
60	68.31	65.58	-4.00
80	32.73	31.9	-2.54
100	23.42	22.3	-4.78
120	20.27	19.5	-3.80

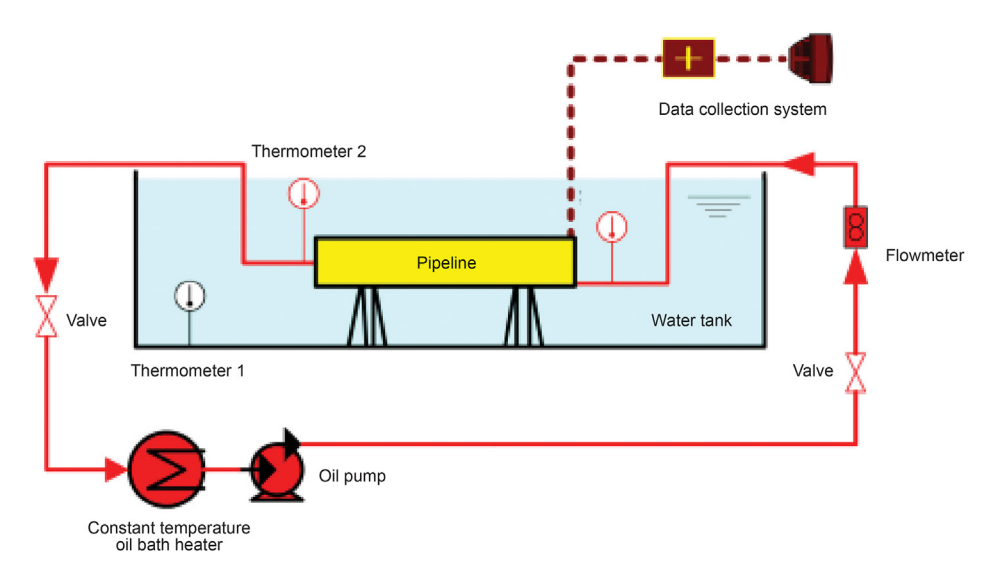


Fig. 14. Layout of insulation test system for oil pipeline.

Fig. 15 shows the actual pipeline of the subsea tree. The inner diameter of the pipeline was 130 mm, and the length was 700 mm. To keep the heat of crude oil from escaping through the ends of the pipeline during the test, we added insulation layers (about 150 mm) to both ends. For the pipe section, at the internal crude oil temperature of 60 $^{\circ}$ C, the thickness of the integral polyurethane insulation layer was 65.58 mm, according to Eq. (19).

Because the axial dimension of the pipeline was not large and its temperature remained almost unchanged in the axial direction, the temperature distribution of certain section could represent the temperature field of the entire pipeline. We monitored the average values of the temperature sensors No. 1–13 on the vertical line of the central section to represent the temperature field inside the pipe. The arrangement of sensors is presented in Fig. 16.

We placed an oil pipeline with a 68.31 mm thick insulation layer in a cold-water environment at 8 °C. After opening the constant temperature oil bath and heating the oil to 60 °C, we turned on the oil pump and monitored the temperature value of the sensor inside the pipeline. When the internal temperature of the oil pipeline

reached 60 $^{\circ}$ C and became stable, we closed the pump and valve. We initiated the collection of temperature drop data when the hot oil circulation was terminated. The frequency of collection was once per 10 s in the first 5 min, once per 30 s after 5 min, once per 1 min after 30 min, once per 5 min after 1 h, once per 10 min after 3 h, and once per 20 min after 5 h. To avoid an increase in the water temperature as a result of the heat dissipation of the pipe during the experiment, we added ice to the tank to keep the water temperature at 8 $^{\circ}$ C.

5.2. Experimental validation

The relative positions 1–7 in Table 6 and Fig. 17 correspond to the measuring points 7, 14–19, respectively. Table 7 and Fig. 18 illustrate the temperature distribution of the measuring points 1 once 13 at the vertical line at different times. Considering the results in Figs. 17 and 18, the temperature at the respective point on the center section decreased rapidly in the first 2 h, and the temperature in the area near the wall declined considerably faster than



(a) No insulation layer added



(b) Add insulation layer

Fig. 15. Oil pipeline of subsea vertical X-mas tree.

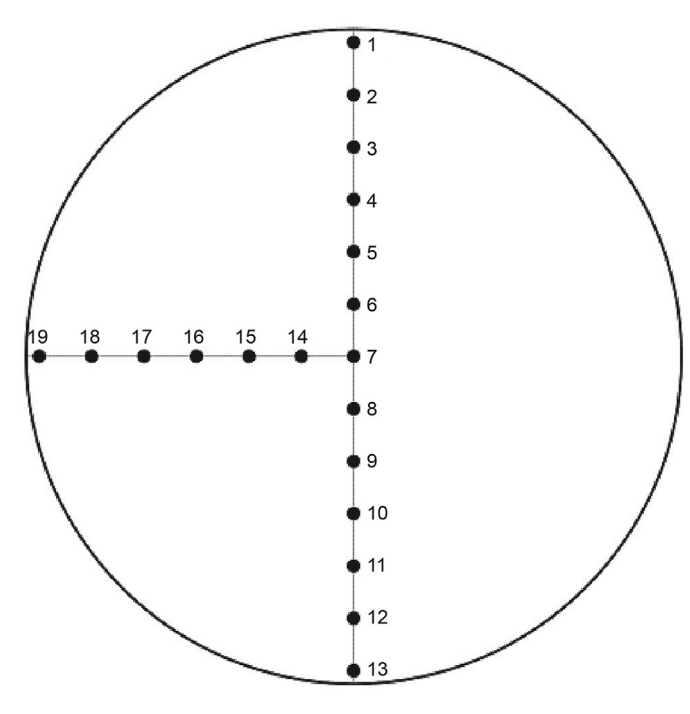


Fig. 16. Location of thermal resistances.

Table 6Temperature of measuring points at the horizontal line at different times.

Relative position	Experimental results, °C					
	0 h	2 h	4 h	6 h	8 h	10 h
1	60.2	42.0	36.7	34.2	32.8	31.1
2	59.9	41.3	35.6	32.6	31.1	29.5
3	60.0	39.8	33.9	30.9	28.5	26.7
4	59.3	38.9	31.4	28.1	26.1	24.4
5	59.5	35.8	29.3	25.3	22.5	20.3
6	58.9	33.4	25.3	19.9	16.6	14.2
7	58.7	29.3	18.9	13.5	9.4	7.1

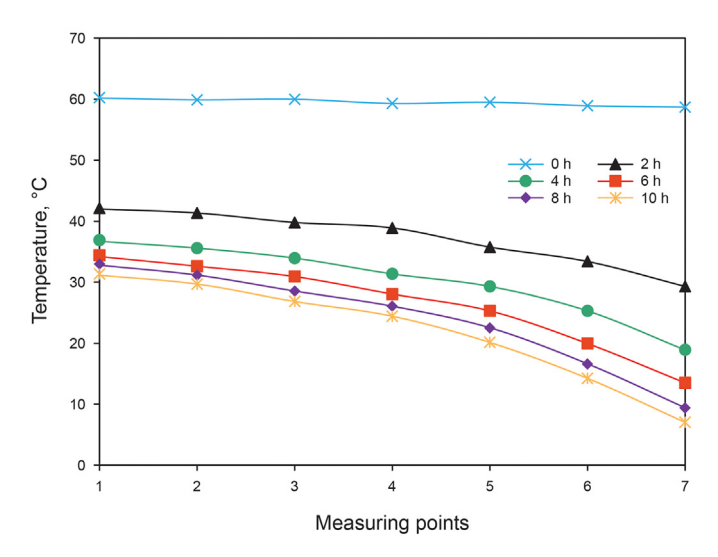


Fig. 17. Temperature of measuring points at the horizontal line.

at the center. After 4 h, the speed of the overall temperature drop tended to be flat.

As shown in Fig. 17, the temperature of the upper half of the center section generally was slightly higher than in the lower half.

Table 7Temperature of measuring points at the vertical line at different times.

Relative position	Experimental results, °C					
	0 h	2 h	4 h	6 h	8 h	10 h
1	58.7	33.9	24.8	16.8	12.0	10.2
2	59.3	37.2	29.7	23.9	18.8	17.0
3	59.5	38.6	32.3	27.8	24.9	23.1
4	60.1	40.6	34.7	31.3	28.9	27.1
5	59.9	40.9	36.1	33.3	31.3	29.5
6	60.0	41.7	36.6	34.2	33.0	31.2
7	60.2	42.0	36.7	34.2	32.8	30.9
8	59.9	41.7	35.4	33.4	31.8	30.1
9	60.0	40.2	33.2	30.8	28.7	26.9
10	59.3	38.7	31.1	27.8	25.8	24.1
11	59.0	36.0	27.8	24.0	20.7	18.8
12	59.3	33.5	24.3	19.2	15.7	13.9
13	58.5	29.2	18.5	13.1	9.2	7.4
T _{Ave}	59.5	38.0	30.9	26.9	24.1	22.3

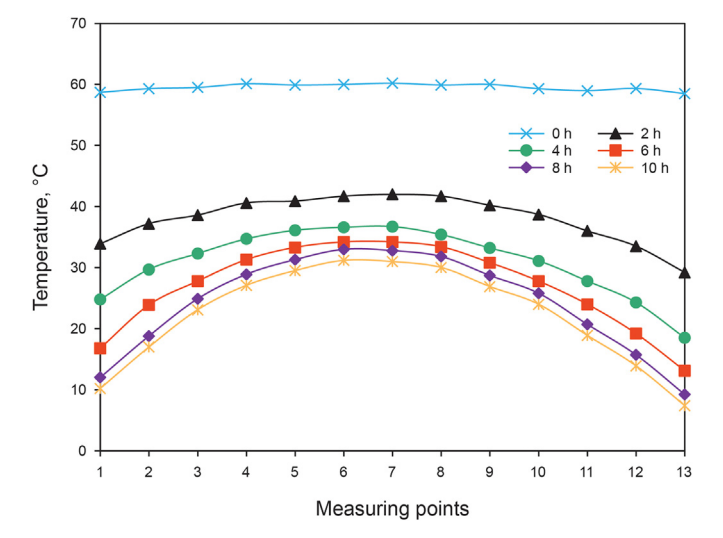


Fig. 18. Temperature of measuring points at the vertical line.

We attributed this to the fact that the temperature difference inside the crude oil gradually increased and led to the formation of a natural convection, thereby resulting in an increase in higher-temperature oil because of the lower density. About 3 h later, the temperature of the bottom zone dropped to the critical value, and the oil began to solidify. After 8 h after shutdown, nearly half of the area reached a temperature below the critical value.

where T_{Ave} is the average values of the temperature sensors No. 1–13.

Table 8 and Fig. 19 the temperature drop of crude oil in the pipeline by experiment and formula calculation. As can be seen, calculation formula predicts the temperature drop process of crude oil with an error below 8.67% compared with experimental results. The formula results showed that the average oil temperature in pipes reached the critical value after 8 h and 43 min. Compared with the calculation result of the empirical formula in Eq. (19), the test result was reached in 43 min, and the error of the empirical formula was 8.96%.

We identified four main causes for the differences between the experimental result and formula calculation. First, the empirical formula was derived based on the results of numerical calculations, whereas the intent heat of phase change released by solidification was not considered in numerical simulation. Second, the external water environment of the test was static, and there was no convective heat transfer. Although the ratio of heat loss resulting

Table 8The temperature drop of crude oil obtained from experiment and calculation.

Time, h	Experimental results, °C	Calculation results, °C	Error, %
0	59.5	60.0	-0.81
2	38.0	36.4	4.44
4	30.9	28.4	8.67
6	26.9	24.9	8.06
8	24.1	23.2	3.89
10	22.3	22.0	1.55

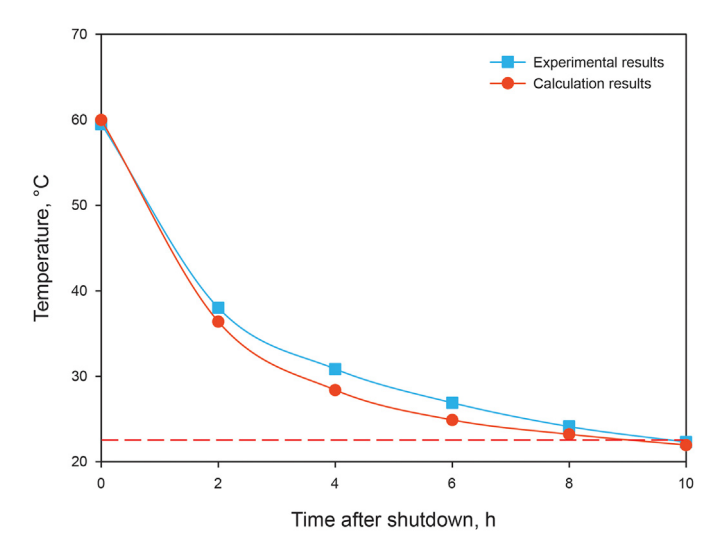


Fig. 19. Temperature drop of crude oil in pipeline.

from external convective heat transfer to the total heat loss was small, the static water still delayed the temperature drop of crude oil to a certain degree. Third, the oil temperature of the empirical formula was characterized by the average body temperature, whereas the oil temperature of the test was characterized by the average value of the temperature measuring point on the vertical line of the central section. Fourth, the experimental error originates from instrument measurements errors. For temperature measurement, the instrument accuracy is 0.28%. Thus, the uncertainty for temperature measurement is around 0.28%. Overall, under the noted limited test conditions, the oil pipeline insulation test verified the feasibility of the empirical formula.

6. Conclusion

We developed a set of insulation design methods for underwater equipment using the thermal insulation design of a subsea vertical X-mas tree. Our main conclusions are summarized as follows:

- (1) The three main steps in thermal insulation design are steady heat transfer analysis, unsteady heat transfer analysis, and derivation of the insulation layer calculation formula. The steady-state analysis obtained the initial temperature conditions for an unsteady calculation and the unsteady-state analysis characterized the relationships between insulation thickness and holding time. For the derivation of the calculation formula, the effect of environmental factors on the insulation enhanced the applicability of the formula.
- (2) For the complex structure of the tree, we selected a singlelayer insulation structure for the heat preservation design. After comparing the properties of different insulation

- materials, we used integral polyurethane as the heat insulating material.
- (3) We also discussed the thermal insulation characteristics of the subsea vertical X-mas tree with different thicknesses of insulation layers under shutdown conditions. The result revealed that the holding time of the insulation increased linearly with an increase in thickness. By analyzing the effects of environmental conditions on the insulation effect, we proved that the initial temperature of crude oil acted as the main factor affecting the duration of insulation layer.
- (4) To verify the feasibility of the empirical formula, we performed an insulation test of the oil pipe. The results demonstrated that the error of the empirical formula was 8.96%, which tended to be conservative. Therefore, this formula can be applied to actual production.

Acknowledgment

This work was financed by the Scientific Research Project of Ocean Engineering Equipment, Ministry of Industry and Information Technology of China.

References

Aarnes, K.A., Lesgent, J., Hübert, J.C., 2005. Thermal design of a dalia SPS deepwater christmas tree-verified by use of full-scale testing and numerical simulations. In: Offshore Technology Conference, Houston, Texas. https://doi.org/10.4043/ 17090-MS.

Bai, Y., Bai, Q., 2019. Overview of Subsea Engineering. Subsea Engineering Handbook (Second Edition), pp. 3–22. https://doi.org/10.1016/B978-0-12-812622-6.00001-4.

Caputo, F., Cascetta, F., Lamanna, G., Rotondo, G., Soprano, A., 2015. Estimation of the damage in a natural gas flow line caused by the motion of methane hydrates. J. Nat. Gas Sci. Eng. 26 (9), 1222–1231. https://doi.org/10.1016/j.jngse.2015.07.050.

Chen, J.Y., Liang, F.H., 2012. Research and development status of thermal insulation materials for deep-water underwater structures. Ship Eng. 34 (1), 87–91. https://doi.org/10.13788/j.cnki.cbgc.2012.01.002.

Chen, X., Mclaury, B.S., Shirazi, S.A., 2004. Application and experimental validation of a computational fluid dynamics (CFD)-based erosion prediction model in elbows and plugged tees. Comput. Fluid 33 (10), 1251–1272. https://doi.org/10.1016/j.compfluid.2004.02.003.

Davalath, J., Hurtado, M., Keig, R., 2002. Flow assurance management for Bijupira and Salema field development. In: Proceedings of the 34th Annual Offshore Technology Conference, 6-9 May, Texas, Houston. https://doi.org/10.4043/ 14052-MS.

Davis, P., Brockhurst, J., 2015. A framework for technology review and selection. Ocean Eng. 1 (104), 540–548. https://doi.org/10.1016/j.oceaneng.2015.04.025.

Dwight, J., Nigel, M., Janardhan, D., 2004. Prediction of cool down times and designing of insulation for subsea production equipment. In: Offshore Technology Conference, Houston, Texas.

Frank, C., McCavitt, B., Brian, S., 2008. Deepwater gulf of Mexico development challenges overview. In: SPE North Africa Technical Conference & Exhibition, 12-14 March, Marrakech, Morocco. https://doi.org/10.2118/113011-MS.

Gao, Z.T., Dai, Z.S., Song, P.N., Chen, X., 2015. Research progress on thermal insulation technology of marine oil pipelines. Jiangsu Shipbuild. 32 (1), 25–27. https://doi.org/10.19646/j.cnki.32-1230.2015.01.008.

Hu, B., Zhu, H., Ding, K., 2015. Numerical investigation of heat transfer characteristics for Subsea Xmas tree assembly. J. Mech. Sci. Technol. 29 (11), 4933–4942. https://doi.org/10.1007/s12206-015-1041-x.

Hu, B., Zhu, H.W., Ding, K., 2016. Numerical investigation of conjugate heat transfer on exterior surfaces of an underwater gate valve assembly. Appl. Ocean Res. 56 (11), 1–11. https://doi.org/10.1016/j.apor.2015.12.006.

Koosha, K., Newsha, E., 2020. Qualitative and quantitative optimization of thermal insulation materials: insights from the market and energy codes. J. Build. Eng. 30, 101–115. https://doi.org/10.1016/j.jobe.2020.101275.

Lei, C., Armfield, S.W., Patterson, J.C., 2008. Unsteady natural convection in a water-filled isosceles triangular enclosure heated from below. Int. J. Heat Mass Tran. 51 (11), 2637–2650. https://doi.org/10.1016/j.ijheatmasstransfer.2007.09.036.

Lu, Y.J., Marotta, E., Skeels, H.B., 2011. CFD thermal analysis of subsea equipment and experimental validation. In: Offshore Technology Conference, 2-5 May, Houston, Texas. https://doi.org/10.4043/21553-MS.

Minami, K., Kurbann, A.P.A., Khalil, C.N., Kuchpil, C., 1999. Ensuring flow and production in deepwater environments. In: Offshore Technology Conference, 3-6 May, Houston, Texas. https://doi.org/10.4043/11035-MS.

Modeste, K.N., Ramaroson, M., 2015. Study of the economical and optimum thermal insulation thickness for buildings in a wet and hot tropical climate: case of

X. Rong and H.-W. Zhu

- Cameroon, Renew, Sustain, Energy Rev. 50, 1192—1202. https://doi.org/10.1016/i.rser.2015.05.066.
- Montazeriab, H., Blockena, B., 2018. Extension of generalized forced convective heat transfer coefficient expressions for isolated buildings taking into account oblique wind directions. Build. Environ. 140 (8), 194–208. https://doi.org/10.1016/j.buildenv.2018.05.027.
- Qin, L.Q., Deng, X.Z., Liu, B., et al., 2011. Ecological risk characterization and assessment of PHAS in the Shengli oil field. Procedia Environ. Sci. 10, 1685–1691. https://doi.org/10.1016/j.proenv.2011.09.265.
 Ratnam, G.S., Vengadesan, S., 2008. Performance of two equation turbulence
- Ratnam, G.S., Vengadesan, S., 2008. Performance of two equation turbulence models for prediction of flow and heat transfer over a wall mounted cube. Int. J. Heat Mass Tran. 51 (11–12), 2834–2846. https://doi.org/10.1016/ i.iiheatmasstransfer.2007.09.029.
- Rivas-Cardona, A., Silva, C., Marotta, E., et al., 2013. Multiphase CFD cool-down behaviors of an EVDT and manifold systems. In: Offshore Technology Conference, 11-14 May. Houston, Texas, https://doi.org/10.4043/24007-ms.
- Shubham, T., Sathvik, D., Michael, M., Christopher, V., Andre, M., 2019. Modeling and dynamic analysis of a mobile underwater turbine system for harvesting Marine Hydrokinetic Energy. Ocean Eng. 187, 106069 https://doi.org/10.1016/j.oceaneng.2019.05.051.

- Singh, A., Sarkar, S., Spritzer, J.M., 2014. CFD based erosion analysis for design of subsea hardware in a high flow rate gas field. In: Offshore Technology Conference, Houston, Texas. https://doi.org/10.4043/24710-MS.
- Sorbye, S., Moe, R., 2006. A system design approach for thermal insulation of subsea equipment using CFD. ASME Conf. Eng. Syst. Des. Anal. 9, 205–214. https:// doi.org/10.1115/ESDA2006-95255.
- Susan, C., Faisal, K., John, S., et al., 2013. Analysis of pitting corrosion on steel under insulation in marine environments. J. Loss Prev. Process. Ind. 6 (26), 1466–1483. https://doi.org/10.1016/j.jlp.2013.09.010.
- Wu, G.Y., 1986. Calculation method of thickness of insulation layer. Guangdong Chem. Indus. 2, 62–67.
- Xu, C., Zhang, Z., Liu, P., Liu, Z., Wang, Q.Z., 2019. Advances in heat preservation technology and application of oil pipelines. China Plastics 33 (11), 99–111. https://doi.org/10.19491/j.issn.1001-9278.2019.11.018.
- Yang, J.D., Zhang, X.L., Wu, W.T., Kong, R.L., Du, B.Y., 2015. Development of composite polyurethane insulation materials for marine oil pipelines. Thermosetting Resin 30 (4), 36–39. https://doi.org/10.13650/j.cnki.rgxsz.2015.04.009.
- Zabaras, G.J., Zhang, J.F., 1997. Steady-state and transient thermal performance of subsea hardware. In: Offshore Technology, Houston, Texas. https://doi.org/10.2118/39122-pa.